Pulse-induced focusing of Rydberg wave packets

D. G. Arbó,[1,2,3] C. O. Reinhold,[2,1] J. Burgdörfer,[1,3] A. K. Pattanayak,[4] C. L. Stokely,[5] W. Zhao,[5] J. C. Lancaster,[5] and F. B. Dunning[5]

[1]*Department of Physics, University of Tennessee, Knoxville, Tennessee 37996-1200, USA*
[2]*Physics Division, Oak Ridge National Laboratory, Oak Ridge, Tennesse 37831-6372, USA*
[3]*Institute for Theoretical Physics, Vienna University of Technology, A-1040 Vienna, Austria*
[4]*Department of Physics and Astronomy, Carleton College, Northfield, Minnesota 55057, USA*
[5]*Department of Physics and Astronomy, and the Rice Quantum Institute, Rice University, MS 61, 6100 Main Street, Houston, Texas 77005-1892, USA*

(Received 13 February 2003; published 13 June 2003)

We demonstrate that strong transient phase-space localization can be achieved by the application of a single impulsive ''kick'' in the form of a short (600 ps) unidirectional electric-field pulse to a strongly polarized, quasi-one-dimensional Rydberg atom. The underlying classical dynamics is analyzed and it is shown that phase-space localization results from a focusing effect analogous to rainbow scattering. Moreover, it is shown that the essential features of the classical analysis remain valid in a quantum-mechanical treatment of the system in terms of its phase-space Husimi distribution. The degree of phase-space localization is characterized by the coarse-grained Renyi entropy. Transient phase-space localization is demonstrated experimentally using extreme redshifted $m=0$ potassium Stark states in the $n=351$ manifold and a short probe pulse. The experimental data are in good agreement with theoretical predictions. The localized state provides an excellent starting point for further control and manipulation of the electron wave packet.

DOI: 10.1103/PhysRevA.67.063401 PACS number(s): 32.80.Rm, 32.80.Qk, 32.60.+i, 42.50.Hz

I. INTRODUCTION

There is much current interest in the control and manipulation of atomic wave functions to generate tailored wave packets [1–3]. Such coherent control promises new opportunities for controlling chemical reactions and has potential applications in, for example, data storage [4]. One important step in this direction is to develop techniques to create electron wave packets that are localized in phase space. In essence, the more tightly an initial state is localized in phase space, the easier it is to produce some desired final state [3,5]. Efforts in this area date back to the early work by Schrödinger [6] where a quantum state was sought which resembled a quasiclassical electron moving in a Kepler orbit. Initial ''gedanken'' experiments were aimed at constructing nondispersive minimum-uncertainty wave packets similar to ''coherent'' oscillator eigenstates. The latter follow Newton's laws of motion, while their widths in position and momentum remain at the minimum consistent with the Heisenberg uncertainty principle. Attempts to generate such electronic states in atoms failed because, in atoms, the energy levels are not equispaced, leading to dephasing, i.e., any phase-space localization of a Rydberg wave packet is transient (without external influence). Nonetheless, even though phase-space localization is transient, such states can be ''trapped'' for extended periods using a train of short unidirectional electric-field pulses, termed half-cycle pulses (HCPs), and later ''released'' simply by turning off the pulses [1]. Similar ideas using microwaves have been proposed and have led to a generalization of the concept of ''nondispersive'' wave packets [5,7]. In both cases, trapping results because the combination of the Coulomb interaction and the external periodic driving field gives rise to sizable stable islands in an otherwise chaotic phase space from which the electron cannot escape.

In this work, we are concerned with the prerequisite of trapping i.e., the creation of a localized state in phase space prior to trapping. We demonstrate that strong transient phase-space localization can be obtained experimentally by the application of a single HCP to a strongly polarized quasi-one-dimensional Rydberg atom. This approach is based on an earlier theoretical analysis of entropy dynamics in classical nonlinear systems [1,8] in a classical Rydberg atom that turned out to be an extension of a scheme introduced previously [3]. We present a detailed analysis of the classical dynamics associated with phase-space localization for both one-dimensional (1D) and three-dimensional (3D) systems and show that localization is a consequence of phase-space focusing in classical Coulomb systems that is analogous to rainbow scattering. In addition, it is shown that the essential features of this classical analysis remain valid in quantum dynamics through 1D quantum calculations based on the time evolution of the Husimi distribution [9] of the nonstationary wave packet. Experimental evidence of transient phase-space localization is presented, which confirms the theoretical predictions.

II. PHASE-SPACE LOCALIZATION IN 1D

Consider initially a 1D hydrogen atom with Hamiltonian

$$H_{\mathrm{at}}=\frac{p^2}{2}-\frac{1}{q} \quad \text{with} \quad q>0, \tag{2.1}$$

where q and p denote the position and momentum of the electron, respectively (atomic units are used throughout this work). Assume that the system is initially in an eigenstate

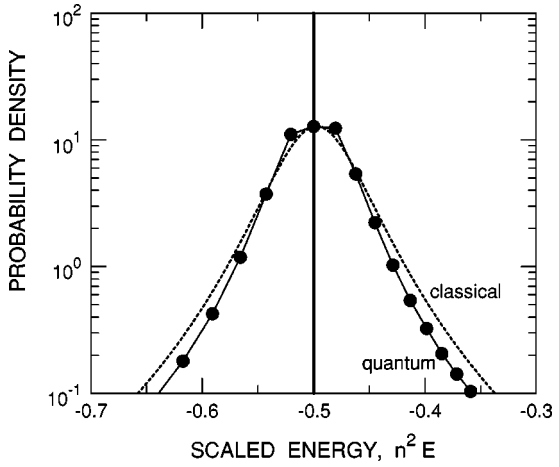

FIG. 1. Final-state energy distribution following the application of a kick with scaled strength $\Delta p_0 = n\Delta p = -0.05$ to a 1D hydrogen atom initially in the $n=50$ state. The vertical line at $E_0 = n^2 E = -0.5$ corresponds to the energy distribution before the kick. Results from both classical (dashed line) and quantum (solid circles connected with solid line) calculations are included.

$|\phi_n\rangle$ of $H_{\rm at}$ with eigenenergy $E_n = -1/(2n^2)$ and that an impulsive momentum transfer or kick of magnitude Δp is applied to the electron at $t=0$ directed toward the origin. The time evolution of the system is described by the Schrödinger equation for the Hamiltonian $H = H_{\rm at} - q\Delta p\,\delta(t)$ whose solution yields

$$|\Psi(t)\rangle = \exp(-iH_{\rm at}t)\exp(iq\Delta p)|\phi_n\rangle. \tag{2.2}$$

The boost operator $\exp(iq\Delta p)$ simply shifts the initial state in momentum space by Δp and, subsequently, the time evolution is governed by the free-evolution operator $\exp(-iH_{\rm at}t)$. In terms of the eigenstates $|\phi_\alpha\rangle$ of $H_{\rm at}$ (i.e., $H_{\rm at}|\phi_\alpha\rangle = E_\alpha|\phi_\alpha\rangle, \alpha = 1,2,\ldots$), the electron wave function evolves in time according to

$$|\Psi(t)\rangle = \sum_\alpha e^{-iE_\alpha t}\langle\phi_\alpha|\exp(iq\Delta p)|\phi_n\rangle|\phi_\alpha\rangle, \tag{2.3}$$

which represents a ''fully coherent'' wave packet, i.e., a pure state at each instant of time [expressed in terms of the density operator $\hat{\rho}$, $\mathrm{Tr}\hat{\rho}^2(t) = \mathrm{Tr}\hat{\rho}(t)$]. Figure 1 shows the final-state energy distribution following the application of a kick that delivers a scaled impulse $\Delta p_0 = n\Delta p = -0.05$ to a 1D ''atom'' initially in the $n=50$ state. For $E<0$, the quantum spectral density is given by

$$\rho^{(Q)}(E=E_\alpha) = \alpha^3|\langle\phi_\alpha|\Psi(t)\rangle|^2 = \alpha^3|\langle\phi_\alpha|\exp(iq\Delta p)|\phi_n\rangle|^2. \tag{2.4}$$

Alternatively, the problem can be described classically using the same Hamiltonians and representing the state of the electron by a probability density in phase space, $\rho^{(C)}(q,p,t)$, that initially ''mimics'' the quantum state and whose dynamics is governed by the classical Liouville equation. A stationary 1D Rydberg atom in a given n level can be represented by a microcanonical phase-space distribution $\rho_n^{(C)}(q,p) = k\delta(H_{\rm at}(q,p) - E_n)$, where k is a normalization constant. Immediately after the kick, at $t=0^+$, this distribution becomes $\rho^{(C)}(q,p,0^+) = k\delta(H_{\rm at}(q,p-\Delta p) - E_n)$ and corresponds to a continuous spectral density

$$\rho^{(C)}(E) = \int dqdp\,\rho^{(C)}(q,p,0^+)\,\delta(E - H_{\rm at}(q,p)) = \frac{(2E_n)^3}{2\pi|\Delta p|}\left[\frac{1}{2}\left(\frac{E_n - (\Delta p)^2/2 - E}{\Delta p}\right)^2 - E\right]^{-2}. \tag{2.5}$$

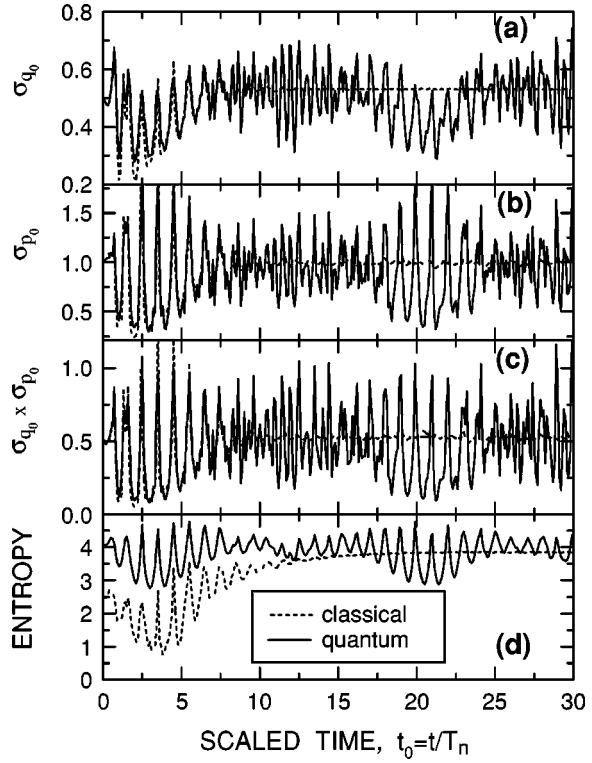

FIG. 2. Time development of various observables following the application of a kick with scaled strength $\Delta p_0 = n\Delta p = -0.05$ to a 1D hydrogen atom initially in the $n=50$ state: (a) scaled width of the position distribution, σ_{q_0}; (b) scaled width of the momentum distribution, σ_{p_0}; (c) scaled effective area occupied by the phase-space distribution, $\sigma_{q_0}\sigma_{p_0}$; (d) the coarse-grained Renyi entropy calculated using a graining $\delta p_0 = 0.1$ and $\delta q_0 = 0.1$. The results are shown as a function of the scaled time $t_0 = t/T_n$.

As is evident from Fig. 1, the predicted classical and quantum spectral densities are very similar. Note that because the system evolves freely after the kick, the energy distribution does not change in time.

The mean value of any observable O adopts the form

$$\langle O\rangle = \sum_{\alpha,\beta} e^{-i(E_\alpha - E_\beta)t}\langle\phi_\alpha|\Psi(0)\rangle\langle\Psi(0)|\phi_\beta\rangle\langle\phi_\beta|O|\phi_\alpha\rangle \tag{2.6}$$

and oscillates in time with frequencies $\omega_{\alpha,\beta} = E_\alpha - E_\beta$. In particular, as shown in Figs. 2(a) and 2(b), the widths of the

momentum and position distributions, $\sigma_q^2=\langle q^2\rangle-\langle q\rangle^2$ and $\sigma_p^2=\langle p^2\rangle-\langle p\rangle^2$, become oscillatory functions of time. The frequency of oscillation is related to the position of the peak in the spectral density, which is located near $E_{peak}=E_n+(\Delta p)^2/2$. Because the scaled impulse Δp_0 is small, the spectral density peaks at $E_{peak}\simeq E_n$ and has a narrow width in both energy and n. In consequence, the frequency spectrum associated with Eq. (2.6) resembles that of a quantum harmonic oscillator [10], i.e.,

$$\omega_{\alpha,\beta}\simeq\omega_n(\alpha-\beta), \tag{2.7}$$

with $\omega_n=n^{-3}$ being the *classical* orbital frequency. This explains why the period of oscillations of σ_q and σ_p in Figs. 2(a) and 2(b) is approximately equal to the orbital period $T_n=2\pi n^3$ (in scaled units, $t_0=t/T_n$, the period is close to unity). At early times, the classical and quantum results mirror each other, i.e., the quantum beats of the system possess a one-to-one correspondence to classical beats, a consequence of the fact that the spectrum for high n locally approximates that of the harmonic oscillator [Eq. (2.7)]. However, the high-n levels are not precisely equispaced. This ''anharmonic'' correction to the frequency spectrum of the wave packet leads to a damping of the quantum beats. Full quantum revivals at times $T_R\simeq(n/3)T_n$ [10] with intermediate fractional revivals at, e.g., $T_R/2$ appear [10,11]. No such revivals are predicted by classical theory due to the continuous classical frequency spectrum.

As is evident from Fig. 2, both σ_q and σ_p minimize simultaneously pointing to transient phase-space localization of the wave packet. The local minima predicted by quantum and classical theories coincide, but the positions of the global minima (i.e., the smallest overall values these quantities achieve) are slightly different. Localization is perhaps visualized more clearly in Fig. 3, which provides snapshots of the classical and quantum probability densities in phase space at different times. To generate the quantum phase-space distributions, we use the Husimi distribution [9]

$$\rho^{(Q)}(q,p,t)=|\langle g(q,p,\sigma)|\Psi(t)\rangle|^2, \tag{2.8}$$

where $|g(q,p,\sigma)\rangle$ is a minimum uncertainty Gaussian wave packet centered at a coordinate q and momentum p, and the squeezing parameter σ is the width of the wave packet in coordinate space (we set $\sigma=n^{3/2}$). Figure 3 shows ''coarse-grained'' histograms, which are constructed by dividing phase space into equally spaced rectangular cells of area $\delta q\,\delta p$ centered at phase-space points $(q_i,p_j)i,j=1,2,\ldots$. The values of the densities displayed in the figure correspond to the average value of the probability density within each cell [12],

$$\rho_{i,j}(t)=\frac{1}{\delta q\,\delta p}\int_{q_i-\delta q/2}^{q_i+\delta q/2}dq\int_{p_j-\delta p/2}^{p_j+\delta p/2}dp\,\rho(p,q,t), \tag{2.9}$$

where we use ρ to represent either the classical or the quantum density ($\rho^{(Q)}$ or $\rho^{(C)}$). Since classical dynamics is scaling invariant, the results are displayed in scaled units $p_0\equiv np$, $q_0\equiv q/n^2$. The times for the snapshots of the densities

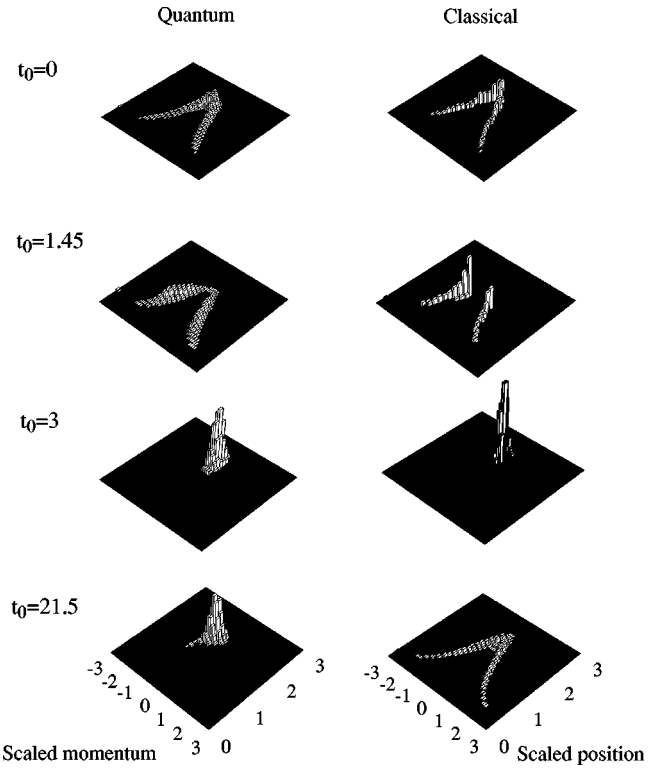

FIG. 3. Quantum (left) and classical (right) coarse-grained phase-space distributions of a 1D hydrogen atom initially in the $n=50$ state ($t_0=0$) and at selected scaled times ($t_0=t/T_n=1.45$, 3, 21.5) following the application of a kick with scaled strength $\Delta p_0=-0.05$. The histograms were obtained using a graining $\delta p_0=0.1$ and $\delta q_0=0.1$.

in Fig. 3 have been chosen using Figs. 2(a) and 2(b) as a guideline. The first snapshot corresponds to the initial electronic state prior to the application of the kick. The classical distribution is somewhat tighter than its quantum counterpart because the former is initially represented by a microcanonical distribution, i.e., a line in phase space, while the latter is represented by a Husimi distribution involving a smooth distribution of binding energies. The second snapshot is for the scaled time $t_0=1.45$, which corresponds to a local maximum in σ_q and σ_p implying, as is observed, that the phase-space density is spread over a broad range of coordinates in phase space. The third snapshot corresponds to $t_0=3$ at which time the quantum calculations predict that σ_q and σ_p will assume their global minimum values. The probability density is concentrated in a small region of phase space implying strong transient localization of the system. The width in phase space is reduced to within a factor $\sim n/10$ of the minimum uncertainty. At late times, the classical-quantum correspondence breaks down. This is illustrated in the fourth snapshot for $t_0=21.5$, which corresponds to a quantum revival (of phase-space localization) and a local minimum in the quantum values of σ_q and σ_p. At this time, the classical distribution has relaxed to an equilibrium phase-space distribution and no localization is evident.

The quantum time evolution of the system is calculated using an expansion of the electronic wave function in a basis set of ~ 300 Sturmian functions [13], which represents a

fraction of both the bound and continuum energy levels. For small kick strengths, as considered here, the continuum does not play an important role and the phase-space distribution is calculated using only the bound spectrum. Similarly, we focus on the classical dynamics of the phase-space density contained in a box $-3<p_0<3$ and $0<q_0<3$ (continuum electrons leave this box quickly). All quantities depicted in Fig. 2 are calculated within this box. The classical Liouville equation determining the dynamics of $\rho^{(C)}$ is solved using a classical trajectory Monte Carlo (CTMC) method: a finite sample of N_{traj} phase-space points distributed according to the initial density is taken and the time evolution of each point is calculated by solving Hamilton's equations of motion. For the 1D hydrogen atom, each point follows a Kepler orbit with maximum eccentricity. The coarse-grained phase-space density can be numerically calculated as

$$\rho_{i,j}^{(C)} = \lim_{N_{traj}\to\infty} \frac{1}{\delta q\,\delta p}\frac{N_{i,j}}{N_{traj}}, \tag{2.10}$$

where $N_{i,j}$ is the fraction of the trajectories lying in the cell centered at (q_i, p_i).

Phase-space localization can be easily visualized within the present 1D model. However, searching for transient phase-space localization in higher dimensions is more difficult. It is therefore desirable to identify a simple functional of the phase-space density that provides a reliable measure of the localization of the system. Such a functional could facilitate the search for improved localization that might be achieved, for example, by using a sequence of tailored electromagnetic pulses. The most natural choice for such a functional in 1D is the product $\sigma_q\sigma_p$ (i.e., the effective phase-space area occupied by the wave packet). This product is depicted in Fig. 2(c) and it obviously provides a satisfactory description of phase-space localization. An interesting alternative is to use entropy as a measure of (de)localization, i.e., of (dis)order, in phase space. This establishes a connection to the statistical mechanics of nonequilibrium systems. In particular, recent work on the dynamics of the coarse-grained entropy of classical ensembles analytically predicts [8] oscillations of the entropy in such systems. The coarse-grained entropy also directly measures the degree to which all the elements of an ensemble behave in a similar fashion, i.e., the degree to which the distribution is localized. Therefore, the coarse-grained entropy can be thought of as measuring the ''statistical coherence'' of the ensemble, whence phase-space localization corresponds to an increase in this statistical coherence. [The term statistical is used here to distinguish this coherence from phase coherence, as exemplified by Eq. (2.3)]. The statistical coherence can be analyzed by considering the time development of the coarse-grained Renyi entropy [8]

$$S_c(t) = -\ln\left[\delta q\,\delta p \sum_{i,j=1}^{\infty} \rho_{i,j}^2(t)\right]. \tag{2.11}$$

It must be emphasized that the coarse-graining of the density is a crucial step in measuring the changes in statistical coherence. In particular, after the kick, because we are considering an isolated system, the classical fine-grained entropy $S_f^{(C)} = -\ln\{\int dqdp[\rho^{(C)}(q,p,t)]^2\}$ is a constant of the motion [14]. It is the division of phase space into finite cells that makes the coarse-grained entropy time dependent. Computing the average density within each cell [Eq. (2.9)] washes out the microscopic information contained in the fine-grained density. For the quantum system, much of the microscopic information is already lost in the calculation of the Husimi distribution, which corresponds to taking a coarse graining of the actual quantum state in phase space, i.e., the Wigner function [9], with a bin size equal to $\hbar$. Quantum coarse graining is therefore mostly due to this Husimi coarse graining rather than Eq. (2.9). Indeed, the statistical coherence or the ''complexity'' of a quantum system could be obtained directly from the Husimi distribution without any additional coarse graining [15,16]. The classical and quantum coarse-grained entropies are displayed in Fig. 2(d) and their minima provide a reasonable measure of phase-space localization.

One drawback of using entropy as a measure of phase-space localization is seen at early times in Fig. 2(d). Unlike the occupied mean phase-space area $\sigma_q\sigma_p$, S_c does not satisfy the correspondence principle: in the limit of short times, classical and quantum Renyi entropies disagree. This discrepancy is due to the different characteristics of the initial probability densities. While the classical initial microcanonical distribution is a δ function (i.e., a line in the 2D phase space), the quantum Husimi distribution is smoother and, consequently, its entropy is higher than the classical one. The ''sharpness'' of the classical distribution is maintained for some time but, finally, it broadens with a consequent increase of the entropy. The differences evident at late times, on the other hand, are to be expected because beyond the characteristic break time, classical-quantum correspondence ceases to hold.

One remarkable feature in Fig. 2(d) is the development of a pronounced narrow maximum in the classical coarse-grained entropy immediately following the global minimum at a scaled time $t_0 \simeq 3$. This pronounced local maximum is universal in the sense that it is observed for any value of Δp_0 (not shown) and is found either immediately preceding or following the global minimum. Moreover, a similar feature is predicted by both the classical and the quantum calculations, albeit shifted in time and less pronounced in the quantum case. The region near the (classical) global minimum is shown in detail in Fig. 4 for a scaled impulse $\Delta p_0 = -0.06$. We now show within the framework of classical dynamics for the 1D system that the global minimum and neighboring sharp maxima are a consequence of the focusing of the phase-space distribution.

In scattering theory, focal points (caustics) lead to singularities in the classical cross sections that are known as rainbow peaks. In the present context, focal points lead to enhancements in the classical phase-space density. For the present problem, rather than searching for a focal point in the 2D phase space, we need only to conduct a 1D search because the spectral distribution (Fig. 1) is narrow and the initial position in the microcanonical ensemble is related one to one to the initial momentum. Specifically, we characterize the ''location'' of the electron within a Kepler orbit at a given

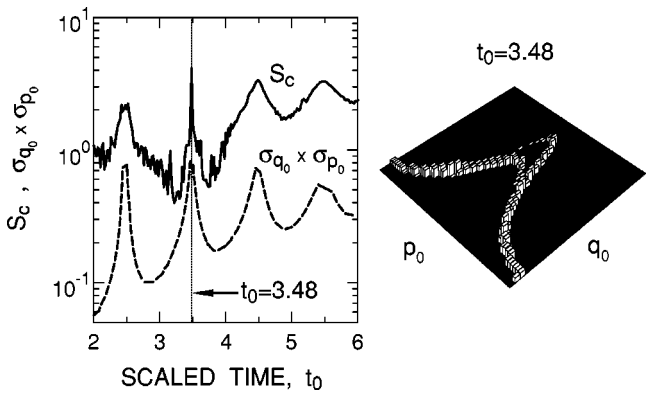

FIG. 4. Time development of the classical coarse-grained entropy (solid line) and the effective area $\sigma_{q_0}\sigma_{p_0}$ (dashed line) following the application of a scaled impulse $\Delta p_0 = -0.06$ to a 1D hydrogen atom initially in the $n=50$ state. The panel to the right shows the coarse-grained classical phase-space distribution at a scaled time $t_0 = 3.48$, which corresponds to the narrow local maximum in the entropy, indicated by the vertical dotted line on the left panel.

time t by an angle variable $\Theta(p_i,t)$ and search for the focusing time t_F by imposing the stationary condition

$$\left.\frac{\partial \Theta(p_i,t)}{\partial p_i}\right|_{t=t_F} = 0. \tag{2.12}$$

At the time t_F, points with different initial values of $\Theta(p_i,0)$ are focused in a region in phase space characterized by the same value of $\Theta(p_i,t)$, though with slightly different "action" (energy).

The location of the electron within a Kepler orbit is unequivocally determined by the angle variable

$$\Theta = \xi - \sin\xi = (-2E)^{3/2}(t+t_i), \tag{2.13}$$

where t_i is given by the phase-space coordinates, immediately after the kick, at $t=0^+$. The angle variable Θ has a one-to-one relation to the time spent in the orbit and is implicitly related to the phase-space coordinates through the eccentric anomaly ξ, and the equations

$$q = \frac{1}{-2E}(1-\cos\xi), \quad p = \sqrt{-2E}\,\frac{\sin\xi}{1-\cos\xi}. \tag{2.14}$$

where $E = H_{\rm at} = p^2/2 - 1/q$.

The explicit dependence of Θ on p_i entering Eq. (2.12) arises from both t_i and E through the set of equations

$$E = E(p_i) = E_n + p_i\Delta p + \frac{(\Delta p)^2}{2}, \tag{2.15}$$

$$(-2E)^{3/2} t_i = \xi_i - \sin\xi_i = \Theta_i, \tag{2.16}$$

$$p_i + \Delta p = \sqrt{-2E}\,\frac{\sin\xi_i}{1-\cos\xi_i}. \tag{2.17}$$

Solving these equations yields

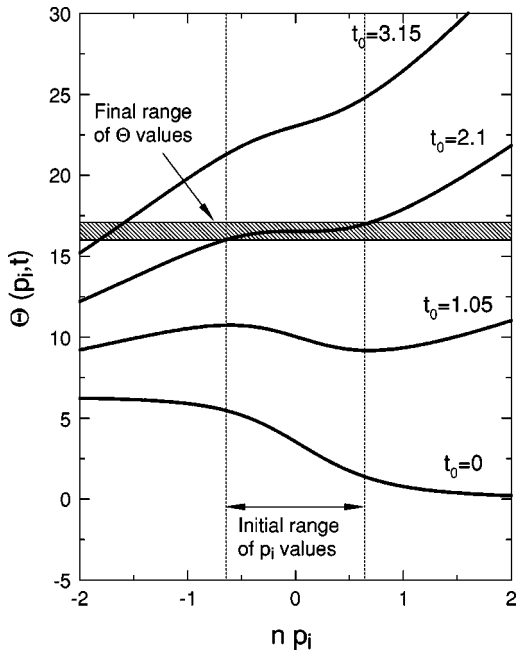

FIG. 5. Dependence of $\Theta(p_i,t)$ on p_i for scaled times $t_0 = 0$, 1.05, 2.1, and 3.15 (see text) following the application of a kick with scaled strength $\Delta p_0 = -0.1$ to a hydrogen atom initially in the $n=50$ state. The vertical lines denote the full width at half maximum of the initial momentum distribution. The shaded horizontal area denotes the final width of the wave packet in the variable Θ.

$$\Theta(p_i,t) = [-2E(p_i)]^{3/2} t + \arccos[A(p_i)] - \sqrt{1-A^2(p_i)} \tag{2.18}$$

for $(p_i+\Delta p) \geqslant 0$ and

$$\Theta(p_i,t) = [-2E(p_i)]^{3/2} t + 2\pi - \arccos[A(p_i)] + \sqrt{1-A^2(p_i)} \tag{2.19}$$

for $(p_i+\Delta p) < 0$, where $A(p_i) = [(p_i+\Delta p)^2 + 2E(p_i)]/[(p_i+\Delta p)^2 - 2E(p_i)]$. Figure 5 illustrates the behavior of the function $\Theta(p_i,t)$ for $\Delta p_0 = -0.1$. At $t_0 = 0$, the angle variable has a monotonic behavior as a function of p_i. The initial width of the wave packet in p_i translates into a sizable width in Θ. At $t_0 = 1.05$, the function $\Theta(p_i,t)$ develops both a maximum and a minimum and, therefore, the stationary condition 2.13 is satisfied for two values of p_i. Subsequently, at $t_0 = 2.1$, the maximum and the minimum merge with each other and become an inflection point (i.e., the second derivative of Θ also vanishes) for $p_i \simeq 0$. At this time, the width of the wave packet in Θ becomes very small. Finally, for times $t_0 > 2.1$, the function $\Theta(p_i,t)$ once again becomes a monotonic function of p_i and focusing disappears.

One key feature of $\Theta(p_i,t)$ is that for $t_0 \simeq 2.1$, it has a weak dependence on p_i since the first and second derivatives vanish. Therefore, an entire range of p_i values is focused onto a narrow range of $\Theta(t_F)$ values. This focusing is the origin of the global minimum. Tight localization in phase space occurs when the electron happens to be near the outer turning point (the apocenter) for times near the focusing time in Θ. Half a period before or after this localization the wave

packet is still focused to a narrow range of Θ values, but these correspond to a collision with the "nucleus." (More generally, in 3D, it reaches the pericenter). The focusing in Θ implies a near simultaneous arrival of the wave packet at the pericenter resulting in a sudden and short-lived broadening and splitting of the momentum distribution as the electrons reverse direction. This broadening of the momentum (and position) distribution is evident in the phase-space density distribution included in Fig. 4 for a scaled time $t_0 = 3.48$ and results in the sharp local maximum immediately following the global minimum. It is worth noting that local density enhancements associated with focusing are accurately mirrored only in the coarse-grained entropy S_c, whereas the mean spread of a wave packet is represented by $\sigma_q \sigma_p$.

Since the focusing in Θ occurs near $p_i \simeq 0$, it is of particular interest to analyze $\Theta(p_i,t)$ in this region. Expanding Eqs. (2.18) and (2.19) to the second order in p_i and Δp yields

$$\Theta(p_i,t) \simeq \pi + \frac{1}{n^3}\left(1 - 3n^2 p_i \Delta p - \frac{3n^2}{2}(\Delta p)^2\right) t - 4n(p_i + \Delta p). \quad (2.20)$$

Imposing now the condition that the angle must be stationary at the focusing point [i.e., Eq. (2.13)] yields

$$t_{F_0} = \frac{t_F}{2\pi n^3} = -\frac{2}{3\pi n \Delta p} \simeq \frac{0.21}{|\Delta p_0|}. \quad (2.21)$$

Note that the quantities in this equation are scaling invariant. Equation (2.21) predicts the optimum focusing time t_F to be inversely proportional to the strength of the kick, $|\Delta p|$. This is confirmed in Fig. 6, which shows that the scaled focusing time t_{F_0}, obtained directly from the global minimum of the classical entropy, is related to the scaled impulse by $t_{F_0} \simeq 0.21/\Delta p_0$. Figure 6 also displays the optimal localization times predicted by quantum calculations. For large impulses, the quantum and classical results are in good agreement. However, in the limit of small kick strengths ($|\Delta p_0| < 0.03$), the results diverge. In this regime, the wavelength associated with the kick, $\lambda \sim 1/|\Delta p|$, becomes larger than the effective size of the wave packet (i.e., $1/|\Delta p| \gtrsim n^2$) and the system cannot be accurately treated classically [17,18].

The focusing time t_F can also be understood in terms of the motion of different parts of the initial ensemble (with small initial p_i values) following the application of a kick. Consider the two points I and II in phase space schematically drawn in Fig. 7 that, prior to the (negative) kick, belong to the same Coulomb orbit with energy $H_{\rm at} = E_n$. Each point was laterally displaced by the same amount Δp by the kick and now propagate on different Kepler orbits that correspond to different energies, $E^j = E_n + (\Delta p)^2/2 + p^j \Delta p$, where $p^j = p^{\rm I}$, $p^{\rm II}$ is the momentum of the electron prior to the kick. Point II corresponds to higher energy than point I and its eccentric anomaly will be larger, i.e., $\Theta^{\rm II}(0^+) > \Theta^{I}(0^+)$. Because point II has higher energy, it moves more slowly in its orbit than point I. Thus, point I can eventually "catch up" with point II giving rise to focusing. Clearly, such catching up can only occur when $\Delta p < 0$.

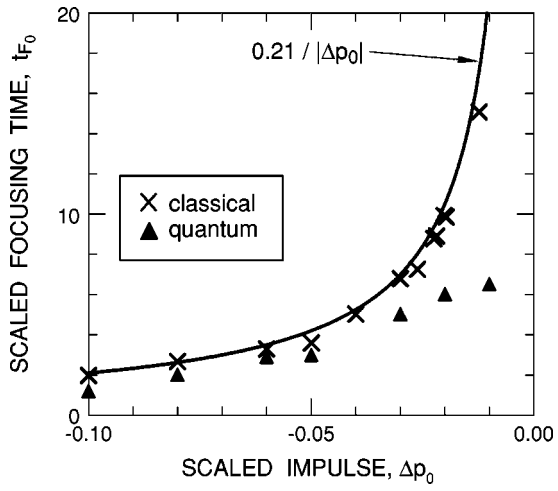

FIG. 6. Dependence of the optimum scaled focusing time t_{F_0} (see text) on the size of the scaled impulse Δp_0 applied to a 1D hydrogen atom initially in the $n = 50$ state. The figure includes the results of classical (crosses) and quantum (solid triangles) calculations and the prediction given by Eq. (2.22) (solid line).

III. PHASE-SPACE LOCALIZATION IN 3D

The first step towards obtaining transient phase-space localization experimentally is the preparation of strongly polarized quasi-one-dimensional Rydberg states. Such states can be produced by photoexcitation of selected Stark states in the presence of a weak dc field [19]. The production of selected Stark states at high n ($n > 100$) is, however, a challenge because the oscillator strengths associated with their

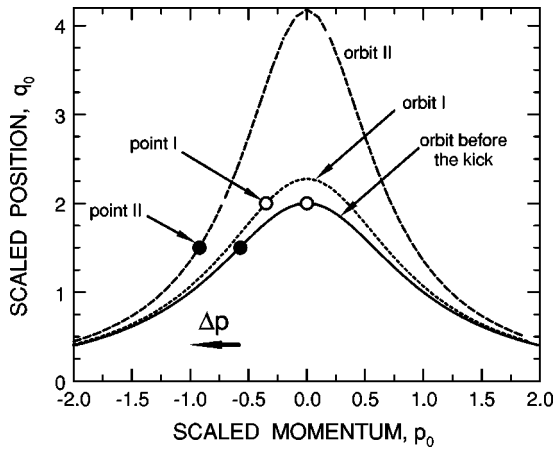

FIG. 7. Diagram showing selected orbits in phase space. Prior to applying the kick, points I (open circle) and II (solid circle) belong to the same initial microcanonical distribution (solid line). After the application of a negative kick Δp, both points are shifted to the left and lie on different Coulomb orbits (dotted and dashed lines).

excitation are small, and because the Stark levels are closely spaced in energy requiring the use of narrow-linewidth frequency-stabilized lasers and tight control of Doppler shifts and broadening. We have recently shown [20] that high-lying quasi-one-dimensional potassium $m=0$ states can be created by photoexcitation of redshifted Stark states in the presence of a weak dc field. This yields a superposition of states whose average dipole moment is large ($z_0=\langle z\rangle/n^2\sim 1.25$), where z is the electron position coordinate along the z axis which is defined to be antiparallel to the dc field.

The apparatus used in this work is described in detail elsewhere [21]. Briefly, ground-state potassium atoms contained in a collimated beam are photoexcited using the output of an extra-cavity-doubled coherent CR 699-21 Rh6G dye laser. The laser is polarized parallel to the applied dc field leading to the creation of only $m=0$ states. Experiments are conducted in a pulsed mode. The output of the (cw) laser is formed into a train of pulses of 1 μs duration using an acousto-optic modulator. Excitation occurs in the presence of a small dc field generated by the application of a small bias potential to a nearby electrode. The uncertainty in the applied field is governed by stray background fields, which can be reduced to $\pm 30\ \mu\mathrm{V\,cm^{-1}}$. Typically strongly polarized redshifted $n=351$ Stark states are excited in a dc field $F_{dc}\sim 300\ \mu\mathrm{V\,cm^{-1}}$. The number of Rydberg atoms produced by each laser pulse is determined by selective field ionization using a ramped field that rises from 0 to $800\ \mathrm{mV\,cm^{-1}}$ in 4 μs.

Transient localization is achieved by applying a short unidirectional HCP. If the duration of the pulse, T_p, is much less than the classical period of the electron, T_n, the HCP simply delivers an impulsive momentum transfer or kick to the electron [17]. The kick, with strength Δp_A, produces a nonstationary wave packet as in the 1D problem discussed in the preceding section. The time development of the wave packet is investigated experimentally by applying a second probe pulse after a variable time delay t_D, and analyzing the behavior of the resulting survival probability as a function of t_D. With a suitable choice of probe pulse, such experiments can provide direct information on the time development of the position and momentum distributions of the electron [21,22]. This is facilitated by the fact that there exists a one-to-one correlation between the local value of the phase-space coordinates of the electron immediately prior to the application of the probe pulse and the energy of the electron after the probe pulse. For example, if $p_z(t_D^-)$ and $E_i=E(t<t_D)$ are the classical momentum and the binding energy of the electron immediately before the application of a probe impulse Δp_B at t_D, the energy of the electron after the probe pulse is

$$E(t>t_D)=E_i+\frac{(\Delta p_B)^2}{2}+p_z(t_D^-)\Delta p_B. \tag{3.1}$$

Therefore, the survival probability, which is given by the fraction of atoms with $E<0$, provides a direct measure of the fraction of electrons with values of $p_z(t_D)$ obeying the inequality

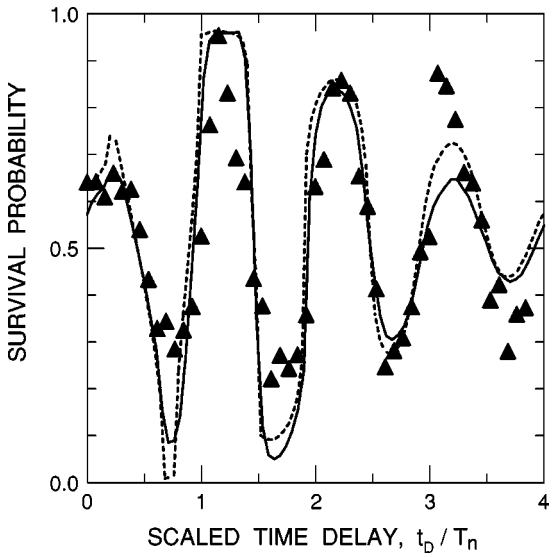

FIG. 8. Survival probability for strongly polarized quasi-one-dimensional potassium atoms in the extreme redmost Stark states in the $n=350$ manifold following the application of a negative pump kick ($n\Delta\vec{p}_A=-0.1\hat{z}$) and a positive probe kick ($n\Delta\vec{p}_B=0.9\hat{z}$) as a function of the scaled time delay t_D/T_n between the pump and probe. Both pulses are applied along the z axis and have a duration $T_p\sim 600$ ps, which is much smaller than the orbital period $T_n=6.5$ ns for $n=350$. The experimental results (solid triangles) are compared with 3D CTMC simulations (solid line) and 1D CTMC simulations (dashed line).

$$p_z(t_D^-)\Delta p_B<-E_i-\frac{(\Delta p_B)^2}{2}. \tag{3.2}$$

Figure 8 shows the time evolution of the survival probability following the application of an initial scaled impulse $n\Delta p_A=-0.1$ when using a probe pulse that delivers a scaled impulse $n\Delta p_B=0.9$. The survival probability undergoes strong periodic oscillations as a function of delay time t_D. Figure 8 includes the results of CTMC simulations for a 1D atom. The remarkably good agreement between these results and the experimental data provides evidence that the dynamics of the experimental system is quasi-one-dimensional. This conclusion can be further tested theoretically by performing 3D CTMC simulations using a collection of strongly polarized states that mimics those initially excited in the experiment, taken to be an incoherent statistical mixture of 36 extreme Stark states belonging to the $n=351$ manifold [20] centered at the peak of the experimental photoabsorption spectrum. As anticipated, the 3D CTMC simulations for such a mixture of states are in very good agreement with the experimental data and the 1D CTMC simulations. Simulations were also performed using a model potential to represent the K^+ core rather than the simple $1/r$ potential. No significant changes in the model predictions were noted, indicating that over the time scale of the present experiments core effects are negligible. The small differences between experiment and theory are probably due to uncertainties in the calibration of the pulsed electric field ($\pm 10\%$) and the impulse it delivers.

Strongly polarized states provide an excellent starting point for producing transiently localized states, since the initial state of the electron is approximately constrained to the two-dimensional (z,p_z) plane. The degree of transient localization of the wave packet produced by the application of a ''pump'' HCP Δp_A can be measured experimentally by subjecting the atoms to a probe pulse Δp_B and observing the survival probability $P_{\rm surv}(\Delta p_B,t_D)$ as a function of both the strength of the probe pulse and the time delay before its application, t_D. Note that $P_{\rm surv}(\Delta p_B,t_D)$ provides an indirect mapping of the momentum distribution as a function of time, $\rho(p_z,t_D)$, because for $\Delta p_B>0$,

$$P_{\rm surv}(\Delta p_B,t_D)\simeq\int_{-\infty}^{(-E_n/\Delta p_B)-(\Delta p_B/2)}dp_z\rho(p_z,t_D), \qquad (3.3)$$

where we have used Eq. (3.2) and the fact that the spectral density is narrow (i.e., $E_i\simeq E_n$). Therefore, information on the time evolution of the wave packet, in particular, its localization in momentum space, can be extracted from $P_{\rm surv}(\Delta p_B,t_D)$. Figure 9 illustrates the behavior of $P_{\rm surv}(\Delta p_B,t_D)$ for the 1D hydrogen atom subjected to a pump kick $n\Delta p_A=-0.1$. A practical approach for estimating the width of the momentum distribution comprises calculating, at a fixed delay time t_D, the difference D_p in the size of the probe impulses required to obtain survival probabilities of 20% and 80%, both of which are indicated in Fig. 9. As demonstrated in Fig. 10, D_p mirrors the behavior of the width of the momentum distribution and provides a measure of the localization of the wave packet in momentum space; the greater the localization, the smaller the range of probe impulses over which the survival probability changes from 80% to 20%. The optimum momentum localization time can be recognized as the one for which the survival probability exhibits the steepest change as a function of the strength of the probe pulse, closely resembling a step function. This result can be understood with the help of Eq. (3.1) and implicitly using the fact that the energy distribution of the electron prior to the application of the probe pulse is very narrow (i.e., the width of the step function is directly related to the width of both momentum and energy distributions).

These considerations indicate that the localization of the wave packet can be investigated experimentally by measuring the survival probability as a function of the size of the probe impulse Δp_B at selected delay times t_D. This is illustrated in Fig. 11, which includes both experimental data and the results of 1D and 3D CTMC simulations. Figure 11(a) shows the survival probability measured with the probe pulse applied directly to the parent state. The survival probability varies relatively slowly with increasing probe strength pointing to a broad range of initial electron momenta, and the data are in excellent agreement with the theoretical predictions. As expected, the survival probability reaches the value $P_{\rm surv}=0.5$ for a scaled impulse $n\Delta p_B\simeq 1$. This occurs because the momentum distribution for the parent state is symmetric around $p_z=0$ and for $n\Delta p_B=1$ all the electrons with

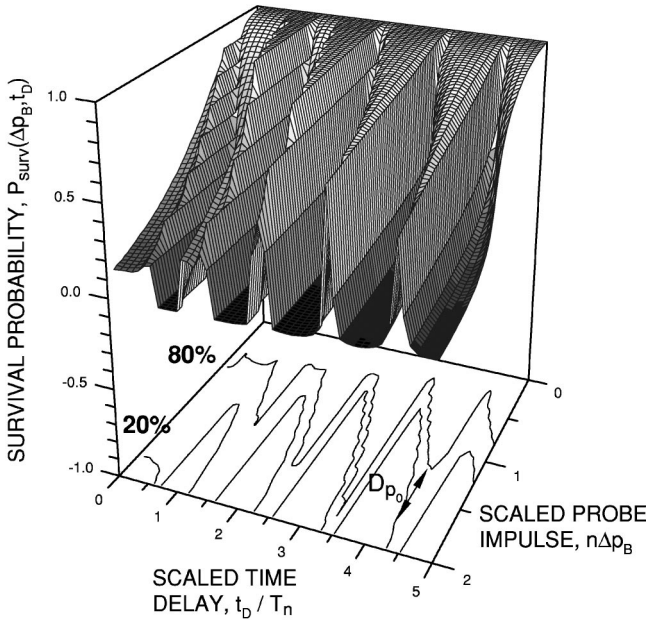

FIG. 9. Survival probability for a 1D hydrogen atom initially in the $n=50$ state following the application of a negative pump kick with strength $n\Delta p_A=-0.05$ and a positive probe kick as a function of the scaled strength of the probe kick, $n\Delta p_B$, and the time delay t_D between the pump and the probe. The lower projections (contours) show the values of $n\Delta p_B$ for which the survival probability is equal to 0.2 and 0.8 as a function of t_D. This is used to obtain the scaled magnitude D_{p_0} shown in Fig. 10.

$p_z>0$ are ionized, whereas those with $p_z<0$ remain bound [see Eqs. (3.1) and (3.3)].

The results in Figs. 11(b) and 11(c) were obtained following the application of a scaled pump impulse $\Delta p_{A_0}=n\Delta p_A=-0.085$. For the data in Fig. 11(b), the probe impulse was applied after a scaled time delay $t_{D_0}=t_D/T_n=1.0$, which is very close to a time at which transient localization is ex-

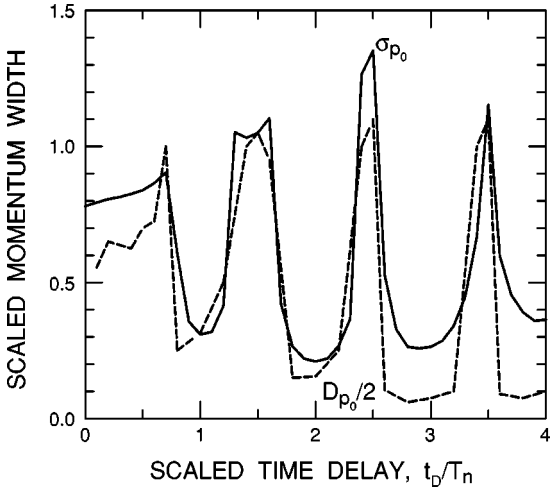

FIG. 10. Comparison of time evolutions of the actual momentum width σ_p (solid line) and the momentum width D_p (dashed line) inferred from the survival probabilities shown in Fig. 9.

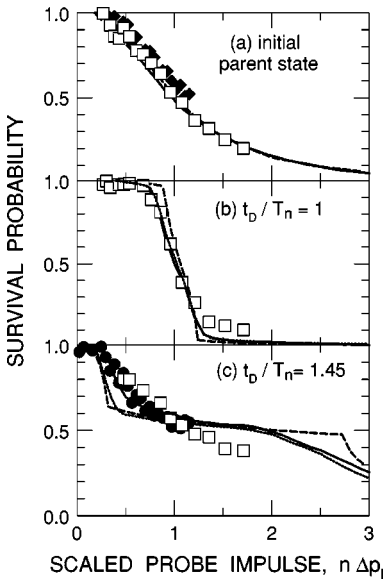

FIG. 11. Survival probabilities obtained using strongly polarized quasi-one-dimensional potassium atoms in the extreme redmost Stark states in the $n=350$ manifold as a function of the scaled strength $n\Delta p_B$ of a probe kick. (a) The probe impulse is applied directly to the initial parent state. (b) The probe kick is applied following a pump kick with $n\Delta \vec{p}_A = -0.085\hat{z}$ and a scaled time delay $t_D/T_n=1$. (c) Same as (b), but for $t_D/T_n=1.45$. The experimental results (symbols) are compared with 1D CTMC simulations (dashed lines) and 3D CTMC simulations using an ultrashort probe pulse (dotted lines) and a probe pulse with a duration of ~ 0.6 ns (solid lines). Experimental data are included for probe pulse durations T_p of ~ 0.6 ns (solid symbols) and ~ 1 ns (open symbols).

pected. The behavior of the survival probability resembles a step function, confirming that momentum localization is indeed occurring. Because the electron energy distribution is narrow, the momentum localization also implies localization of the position coordinates, i.e., the steplike behavior evident in Fig. 11(b) is unequivocally a signature of phase-space localization. In principle, spatial localization can be examined using a field step as a probe [21]. Assuming that the wave packet is localized and that a field step with magnitude F and rise time $t_r \ll T_n$ is applied, the survival probability changes from unity to zero depending on whether $\langle E_i \rangle + F\langle z \rangle < -2\sqrt{F}$ or $\langle E_i \rangle + F\langle z \rangle > -2\sqrt{F}$, respectively, where $-2\sqrt{F}$ represents the top of the potential barrier generated by the field. In practice, however, experiment and theory showed that the survival probability is not very sensitive to variations in the size of the field step indicating that measurements using a probe impulse provide a better indication of localization.

The data in Fig. 11(c) were recorded after a scaled delay time $t_{D_0} = t_D/T_n = 1.45$ when the phase-space distribution is expected to be localized in two different regions (such as shown in Fig. 3), one corresponding to the electron having a sizable positive momentum, the other a sizable negative momentum. Scaled probe impulses $n\Delta p_B \gtrsim 0.3$ are sufficient to ionize that part of the distribution which corresponds to positive electron momenta, whereas impulses $n\Delta p_B \gtrsim 2.7$ are required to ionize the component that corresponds to negative electron momenta. This gives rise to the ''double-step'' structure evident in the calculations using an ultrashort probe pulse. This behavior is not as apparent in the experimental data that are for a probe pulse with a duration of $T_B \simeq 0.6$ ns. This can be attributed to the fact that the electron momentum changes rapidly as it reverses direction at the nucleus. This leads to dramatic changes in the electron momentum distribution, which occur on time scales $\lesssim 0.1 T_n$ (i.e., on time scales $\simeq 0.65$ ns). The measurements are therefore sensitive to the pulse width and this leads to a broadening of the predicted steplike features. The experimental data are however in agreement with CTMC calculations for a 0.6 ns wide probe pulse.

IV. CONCLUSIONS

The present work demonstrates that strong transient phase-space localization can be achieved by the application of a single kick to strongly polarized quasi-one-dimensional Rydberg atoms, providing an ideal starting point for further quantum control and manipulation of electronic wave packets. The experimental observations are in good agreement with the predictions of both classical and quantum theories. Analysis shows that localization can be explained in terms of a focusing effect predicted by classical dynamics. Furthermore, it is demonstrated that the degree of localization (or statistical coherence) can be characterized both by the product of the position and momentum widths and by the coarse-grained Renyi entropy. Work is now underway to examine if the degree of localization can be further enhanced using a sequence of tailored electromagnetic pulses.

ACKNOWLEDGMENTS

This research was supported by the NSF under Grants Nos. PHY-0096392 and PHY-0099504 and by the Robert A. Welch Foundation. D.G.A. and J.B. acknowledge support by the SFB 016 ADLIS of the FWF (Austria). C.O.R. acknowledges support by the OBES, U.S. Department of Energy to ORNL which is managed by the UT-Batelle LLC under Contract No. DE-AC05-00OR22725. A.K.P. acknowledges partial support from the Research Corporation.

[1] C.L. Stokely, F.B. Dunning, C.O. Reinhold, and A.K. Pattanayak, Phys. Rev. A **65**, 021405 (2002).
[2] R.R. Jones and L.D. Noordam, Adv. At., Mol., Opt. Phys. **38**, 1 (1998).
[3] J. Bromage and C.R. Stroud, Phys. Rev. Lett. **83**, 4963 (1999).
[4] T.C. Weinacht, J. Ahn, and P.H. Bucksbaum, Nature (London) **397**, 233 (1999).
[5] A. Buchleitner, D. Delande, and J. Zakrzewski, Phys. Rep. **368**, 409 (2002); A. Buchleitner and D. Delande, Phys. Rev. Lett. **75**, 1487 (1995).

[6] E. Schrödinger, Naturwissenschaften **14**, 664 (1926).
[7] A.F. Brunello, T. Uzer, and D. Farrelly, Phys. Rev. Lett. **76**, 2874 (1996).
[8] A.K. Pattanayak and P. Brumer, Phys. Rev. E **56**, 5174 (1997); A. K. Pattanayak, Physica D **148**, 1 (2001).
[9] K. Husimi, Proc. Phys. Math. Soc. Jpn. **22**, 264 (1940); M. Hillery *et al.*, Phys. Rep. **106**, 121 (1984).
[10] J.A. Yeazell and C.R. Stroud, Phys. Rev. Lett. **60**, 1494 (1988); J. Parker and C.R. Stroud, *ibid.* **56**, 716 (1986); Z.D. Gaeta and C.R. Stroud, Phys. Rev. A **42**, 6308 (1990).
[11] S.D. Boris, S. Brandt, H.D. Dahmen, T. Stroh, and M.L. Larsen, Phys. Rev. A **48**, 2574 (1993); J.E. Bayfield, *Quantum Evolution, an Introduction to Time-dependent Quantum Mechanics* (Wiley, New York, 1999).
[12] R. Tolman, *The Principles of Statistical Mechanics* (Dover, New York, 1979).
[13] M. Rotenberg, Ann. Phys. **19**, 262 (1962); M. Rotenberg, Adv. At. Mol. Phys. **6**, 233 (1970).
[14] Strictly speaking, the fine-grained entropy for a microcanonical ensemble is infinite. This peculiarity can be overcome by changing the initial distribution to a new form in which the Dirac delta function $\delta(H_{at}-E_n)$ is replaced by a function $f(H_{at})$ that peaks at E_n and has a narrow but finite width.
[15] A. Sugita and H. Aiba, Phys. Rev. E **65**, 036205 (2002).
[16] K. Takahashi, Prog. Theor. Phys. Suppl. **98**, 109 (1989).
[17] C.O. Reinhold, M. Melles, H. Shao, and J. Burgdörfer, J. Phys. B **26**, L659 (1993).
[18] C.O. Reinhold and J. Burgdörfer, J. Phys. B **26**, 3101 (1993).
[19] T.F. Gallagher, *Rydberg Atoms* (Cambridge University Press, New York, 1992).
[20] C.L. Stokely, J.C. Lancaster, F.B. Dunning, D.G. Arbó, C.O. Reinhold, and J. Burgdörfer, Phys. Rev. A **67**, 013403 (2003).
[21] B.E. Tannian, C.L. Stokely, F.B. Dunning, C.O. Reinhold, and J. Burgdörfer, Phys. Rev. A **64**, 021404(R) (2001); B.E. Tannian, C.L. Stokely, F.B. Dunning, C.O. Reinhold, S. Yoshida, and J. Burgdörfer, *ibid.* **62**, 043402 (2000).
[22] R.R. Jones, Phys. Rev. Lett. **76**, 3927 (1996); C.O. Reinhold, J. Burgdörfer, M.T. Frey, and F.B. Dunning, Phys. Rev. A **54**, R33 (1996).